Evolution of Marangoni Thermo-Hydrodynamics Within Evaporating Sessile Droplets

Arnov Paul and Purbarun Dhar

Nomenclature

V	Velocity (m/s)
P	Pressure (Pa)
T	Temperature (T)
D	Diffusity of water in air (m^2/s)
K	Thermal conductivity (W/mk)
t	Time (s)
ρ	Density (kg/m^3)
μ	Viscosity ($N.s/m^2$)
L_h	Latent heat of vaporization (J/kg)
R	Universal gas constant (J/mol.k)
β_T	Thermal expansion coefficient (K^{-1})
M	Molecular weight (kg/mol)
c	Concentration (kg/m^3)
J	Evaporative flux (kg/m^2s)
θ_0	Initial contact angle of droplet (°)
γ	Surface tension (N/m)
T_a	Overall temperature inside droplet (K)
V_a	Overall velocity inside droplet (m/s)
γ_T	Temperature co-efficient of surface tension (Nm/K)
a,w (subscript)	Air and water phase

A. Paul (✉) · P. Dhar
Department of Mechanical Engineering, Hydrodynamics and Thermal Multiphysics Lab (HTML), Indian Institute of Technology Kharagpur, Kharagpur 721302, India
e-mail: arnov0381@gmail.com

K. M. Singh et al. (eds.), *Fluid Mechanics and Fluid Power, Volume 5*, Lecture Notes in Mechanical Engineering, https://doi.org/10.1007/978-981-99-6074-3_14

1 Introduction

Evaporation of sessile droplets continuous to be a topic of ongoing research because of its relevance to many natural processes and modern practical applications in the field of heat and mass transfer. Among natural processes, it plays a crucial role in fog, dew and, rain formation mechanism [1, 2]. It is also relevant to other practical applications such as inkjet printing [3], spraying of pesticides [4], anti-icing/ anti-fogging devices in automobile and air crafts [5]. Also, many modern micro scale processes [3, 6] require precise control over deposition pattern of dissolve solute particles which in turn depends on internal advection of liquid molecules during evaporation. Moreover, when the internal flow field is strong enough to induce Stefan flow in the gaseous domain due to shear at the liquid–vapour interface, it may modulate the evaporation process itself as discussed in literature. Hence, an in-depth knowledge about the evaporation mechanism and associated fluid flows of drying droplets under different conditions is of immense importance for efficient designing and development of practical droplet-based devices.

2 Literature Review and Objective

In general, based on shape and geometry droplet literature is broadly classified into sessile and pendant droplets. A pendant droplet simply suspends in a gaseous medium, and evaporation takes place uniformly at a rate proportional to droplet diameter [7]. Whereas a sessile droplet, resting over a solid substrate remains in equilibrium with the gaseous phase surrounding it. The evaporative behaviour of such droplets is more complex, influenced by wetting properties of liquid, three-phase interaction [8], ambient conditions [9, 10], geometry [11–13] and thermo-physical properties [14] of the underlying solid substrate. For instance, a sessile droplet evaporates mostly via constant contact radius mode on high surface energy substrates where for the super-hydrophobic (SH) surfaces constant contact angle mode or mixed mode of evaporation is noticed [8]. These different modes of evaporation may significantly affect the internal advection of fluid particles. In case of pinned contact line over hydrophilic surfaces an outward radial flow was reported by Deegan et al. [15]. This flow is mainly generated due to replenishment the liquid that is being removed from the edge of droplet due to higher evaporative flux near the three-phase contact line. This outward flow of liquid plays a crucial role in transporting dissolved solute particles towards the periphery (forming coffee stain rings).

In addition to wetting state, the internal advection dynamics of a drying drop is dictated by a number of factors such as direction of heat flow from substrate [16], geometrical parameters [17], and thermal effects [18]. For instance, the altered wetting state on curved surfaces can appreciably modulate the internal flow field depending upon the nature of curvature. For a concave surface the circulation strength is mitigated whereas the same is strongly intensified on convex geometry [17].

On heated surfaces [18], the temperature distribution inside droplet is substantially modulated due to the influence of evaporative cooling. This tampered temperature profile may generate buoyancy driven advection or thermal Marangoni flow which ultimately modify the magnitude and pattern of the internal circulation velocity. Also, the strength of internal circulation may be appreciably controlled when droplets are seeded with suitable buoyant particles and external non-tactile body forces (such as electric and magnetic fields) are present in the system [19]. This internal hydrodynamics when sufficiently intensified may itself affect the evaporation mechanism. In such cases, the strong circulation velocity generates shear at the interface which ultimately results in displacing the vapour filed layer with the fresh air in the gaseous domain thus augmenting the evaporation rate [19].

The brief literature summarized above substantiates the influential role of wetting state and substrate temperature on the internal advection of drying droplets. The above discussion also put forward the strong dependence of the evaporation mechanism on the internal hydrodynamics. However, only a few works have addressed the internal flow pattern during the evaporation process in transient stage despite the same may occupy a large fraction of the droplet lifetime. For instance, Maatar et al. [20] showed that the transient state accounts for 80% of droplet lifetime in evaporation of 3-methylpentane droplets on heated surfaces while in isothermal conditions it occupies about 33% of the evaporation time [21]. Recently, Chen et al. [22] probed the internal advection pattern during initial transient regime of rapidly evaporating droplets. However, none of the previous studies analysed the role of contact angle on transient evolution of internal circulation strength of an evaporating sessile droplet. In present study, we numerically model the internal flow field and corresponding temperature profile during the transient stage of an evaporating water droplets for different wettability conditions. The droplet volume is considered to be identical while the contact angle is varied over a wide range to mimic the geometry of a sessile droplet over substrates having different surface energies. The governing differential equations for the transient heat and mass transfer phenomenon are numerically solved in fully coupled manner to investigate the evolution of internal flow field and corresponding temperature distribution.

3 Mathematical Formulation

3.1 Governing Equations

We consider an axisymmetric water droplet with pinned contact line evaporating in quiescent ambient as shown in Fig. 1. The transient problem is mathematically formulated in axisymmetric *r-z* coordinate system based on Arbitrary Lagrangian–Eulerian (ALE) framework [23] with the following assumptions:

- The fluid flow is laminar and incompressible.

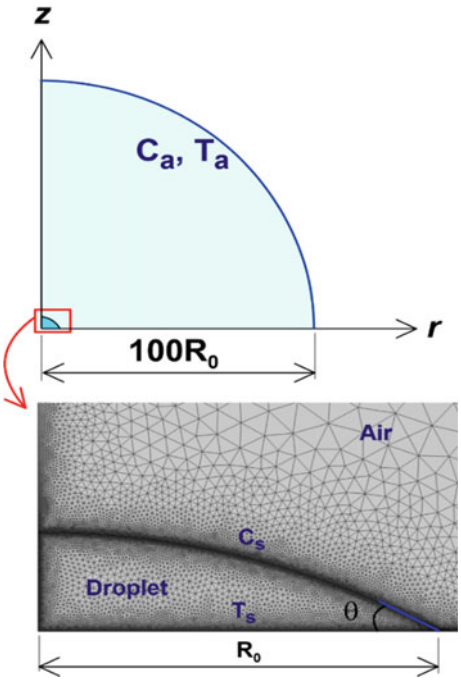

Fig. 1 Schematic and meshing of the computation domain for droplet-ambient system in *r*-*z* coordinate

- Droplet contact line is pinned.
- The thermo-physical properties of fluids are constant unless explicitly specified such as temperature variation of density and surface tension.

Under these conditions the continuity and momentum eqn. in liquid and gas phase is given as:

$$\nabla . V = 0 \tag{1}$$

$$\rho\left(\frac{\partial V}{\partial t} + (V_c.\nabla)V\right) = \nabla\left[-pI + \mu\left(\nabla V + (\nabla V)^T\right)\right] + F_g \tag{2}$$

where ρ, μ, p, t, g are density, viscosity, pressure, time and gravitational constant, V_c is the convection velocity defined as difference between mesh velocity and material velocity in ALE framework, $F_g = (\rho_r + \Delta\rho)g$ is the gravity force that depends on change in density brought about by change in temperature in liquid phase: $\Delta\rho = \beta_T \rho_{w,r}(T - T_r)$, where β_T is thermal expansion coefficient, T is the temperature, and subscript w and r denotes water phase and reference state. In present study, the ambient condition is considered as the reference state. For gaseous phase, density is a function of both temperature and vapour concentration given as:

$$\Delta\rho = \left(\frac{p_a M_a}{RT} + cM_w\right) - \left(\frac{p_{a,r} M_a}{RT_r} + c_r M_w\right) \tag{3}$$

where $p_a = p_o\text{-}cRT$ is partial pressure of air, p_o is total atmospheric pressure, c is the molar vapour concentration, R is the universal gas constant and M_a and M_w is molar mass of air and water respectively. To model the natural convection phenomenon, Boussinesq approximation is used assuming change in density does not tamper the incompressible flow assumption [24]. The mass diffusion at liquid–vapour interface is govern by convection–diffusion eqn. given as:

$$\frac{\partial c}{\partial t} + (V_c.\nabla)c = \nabla[D\nabla c] + S \tag{4}$$

where D is the vapour diffusion coefficient and S is source term for the concentration. In the present study, $S = 0$.

The heat transport eqn. in liquid and gas phase is given as:

$$\rho\left(\frac{\partial T}{\partial t} + (V_c.\nabla)T\right) = \nabla[k\nabla T] \tag{5}$$

where C_p is specific heat and k is the thermal conductivity.

3.2 Initial and Boundary Conditions

We apply constant temperature boundary condition at solid–liquid interface and at far ambient denoted as T_s and T_a respectively. In present study we consider $T_s = T_a = 15$ °C. The liquid–vapour interface is in saturated vapour condition (C_s) while the far field ambient has a relative humidity Φ. We apply no slip boundary condition for velocity and no penetration condition for vapour across the solid–liquid interface for liquid domain and gaseous domain respectively. The initial numerical values of velocity, temperature and relative humidity in present study is consider as 0 m/s, 15 °C, and 50% respectively.

Next, we apply stress balance in normal and tangential direction across the liquid–vapour interface:

$$(\vec{n}\cdot\sigma_a - \vec{n}\cdot\sigma_w)\cdot\vec{n} = {}^{\gamma}\!/_{r_o}\cdot\vec{n} \tag{6}$$

$$(\vec{n}\cdot\sigma_a - \vec{n}\cdot\sigma_w)\cdot\vec{t} = -\gamma_T\nabla_g T \tag{7}$$

where $\nabla_g = (I - \vec{n}\cdot\vec{n}^T)\nabla$ is the surface gradient operator, γ, σ, $\vec{t}$, $\vec{n}$, r_o, γ_T are the surface tension, stress tensor, unit vector along tangential and normal direction, overall curvature radius and temperature coefficient of surface tension respectively.

Next, we apply the mass balance across liquid–vapour interface since the same cannot store any mass given as:

$$V_g - V_l = J\left(\frac{1}{\rho_w} - \frac{1}{\rho_a}\right) \tag{8}$$

$$J = \vec{n} \cdot \left(-D\nabla c + V_g \cdot c\right) M_l \tag{9}$$

where V_g, V_l is the velocity in gas and liquid phase and J is evaporative mass flux. This evaporated liquid mass takes away latent heat of vaporization. As a result, the liquid–vapour interface acts as heat sink for the internal liquid given as:

$$n\left(k_g(\nabla T)_g - k_l(\nabla T)_l\right) = -JL_h \tag{10}$$

where L_h is the latent heat of vaporization.

3.3 Numerical Scheme

The governing equations along with the boundary conditions are numerically solved in a fully coupled manner using commercial software COMSOL Multiphysics 4.4 that provides iterative solution based on finite element method. The discretization in the finite element formulation was done using Lagrange linear shape elements for both velocity and pressure fields. The meshing operation was performed using triangular mesh with the finest mesh size (about 200 times finer than contact radius) being located near the liquid–vapour interface and at the contact line (see Fig. 1). These considerations ensure accuracy in solving heat and mass transport equations and surface tension gradient. The computation domain is considered to have a radius of 100 times the initial radius of droplet as shown in Fig. 1. Moreover, an automatic remeshing operation was adopted to reduce the mesh distortion during evaporation process. In present study, the minimum mesh quality was set to 0.2. The tolerance value was set at 0.001 for all variables. For the grid independent test, we vary the grid numbers from 19,067 to 33,167 and the change in evaporation rate was less than 0.08%.

The validation of the above model is done by comparing present results with the experimental observations of Paul et al. [11] as shown in Fig. 2. We simulate the droplet evaporation problem following two approaches: (i) No internal advection: we neglect the advection of fluid in the mass transport equation and hence the process is considered as diffusion driven evaporation; (ii) With internal advection (IA): we take into account the transport of fluid particles due to buoyancy effects and Marangoni advection. It is noticed that, the advection model predicts the instantaneous droplet volume more accurately while the no advection model under predicts the evaporation rate.

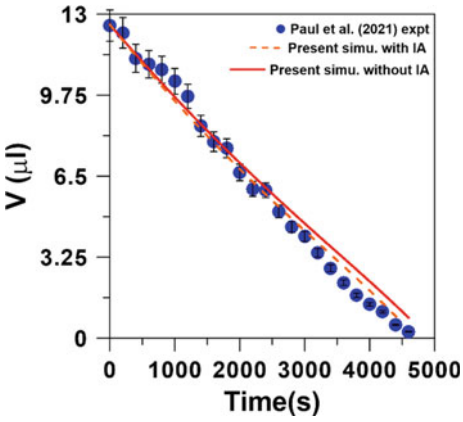

Fig. 2 Comparison of present numerical model with the experimental results on transient droplet volume

4 Results and Discussion

4.1 Temporal Variation of Internal Velocity Field and Temperature Distribution

Figure 3 illustrates the spatial distribution of the internal circulation velocity and corresponding thermal contours inside a sessile droplet at different time instants. It is observed that, on hydrophilic surfaces (initial contact angle, $\theta_0 = 30°$), multiple vortices (multi-vortex pattern) are formed during initial transient regime of evaporation before the internal flow pattern becomes time invariant. In this stage, the total number of vortices firstly increases to maximum value at $t = 4$ s, then reduces to a stable value (single vortex) at latter stages. The final stable vortex consists of a large recirculating flow entraining liquid particles from the peripheral region to the apex along liquid–vapour interface. These findings behind the dynamic evolution of the circulation flow may be attributed the internal thermal imbalance generated due to evaporation of droplets. The diffusion model predicts the evaporative flux to be maximum near the contact line for a sessile droplet evaporating over hydrophilic surfaces [15]. As a result, the liquid–vapour interface at peripheral region is cooled to a greater extent at the very beginning of evaporation ($t = 0.3$ s). This thermal disparity due to evaporative cooling may cause thermal Marangoni flow and buoyancy driven advection. However, the convection patterns due to these two mechanisms are opposite to each other. Initially, the relatively cold fluid at liquid–vapour interface descends towards the periphery while the hotter fluid from the droplet bulk moves upward due to buoyancy. This condition triggers interfacial advection of fluid from to the apex to periphery (as observed at $t = 0.3$ s). However, as evaporation progress, the temperature gradient at the liquid–vapour interface sets off Marangoni advection that entrains liquid from the peripheral region to the apex. These two counteracting flow mechanisms are responsible for generation of vortex flows during the transient regime of evaporation. With progressing time, the non-uniform evaporative flux along

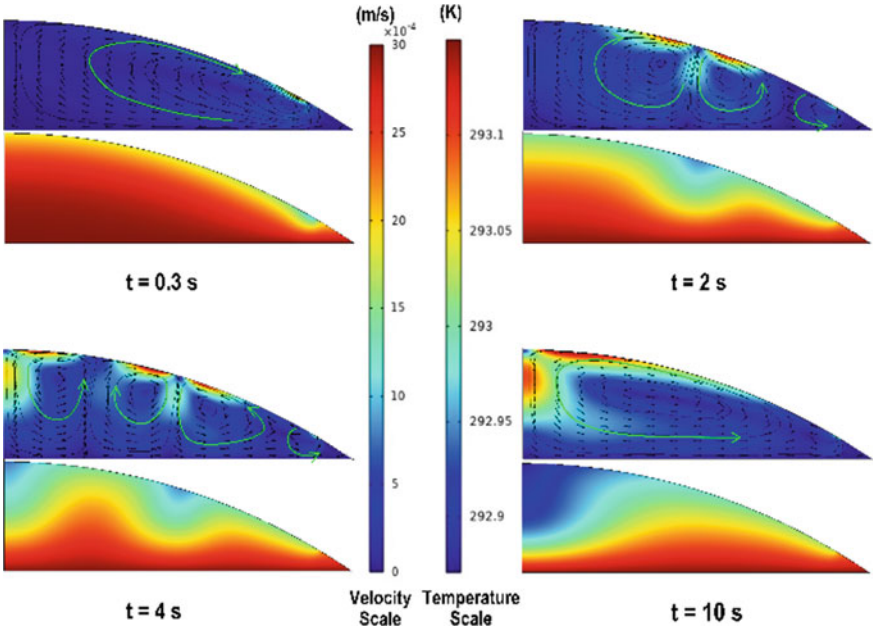

Fig. 3 Transient evolution of the internal velocity field and corresponding temperature distribution of a sessile droplet evaporating over hydrophilic surfaces ($\theta_0 = 30°$)

the internal convective flow cause multiple local maxima in interfacial temperature. These temperature extrema at different locations give rise to local thermal Marangoni cells which ultimately result in formation of multiple vortices as observed at $t = 4$ s in Fig. 3. This local distribution of vortices is advantageous for bulk motion of liquid and hence felicitate the mixing process at initial transient regime.

Finally, at latter stages ($t = 10$ s) the temperature distribution becomes monotonically decreasing along liquid–vapour interface from the contact line to central region. As a result, the Marangoni convection becomes unidirectional along decreasing temperature thus forming single recirculation flow (one vortex pattern) inside the droplet. These observations at this stable condition are in line with the previous studies on internal circulation behaviour of droplets at steady state [16]. Also, it is noticed that the internal temperature at the stable state ($t = 10$ s) is unevenly distributed at different vertical and horizontal locations with the colder fluid mass being at the top central region. Hence, buoyancy-driven advection may have significant role in the overall internal circulation flow in addition to Marangoni convection.

Figure 4 shows the transient variation of internal velocity field and corresponding temperature distribution of an evaporating sessile droplet over SH surfaces (initial contact angle, $\theta_0 = 150°$). It can be noticed that at very beginning (i.e. when the convection current is negligible) the temperature at the apex region is reduced to a

greater extent due to large evaporative flux resulting from diffusion driven evaporation [15]. This cooling effect remains localized at the central core and thus induces liquid motion in the central vertical column due to buoyancy effects (as observed at $t = 0.5$ s). However, the effect of thermal Marangoni flow during this initial regime is relatively small due to little variation in temperature along liquid–vapour interface (as seen in $t = 0.3$ and 0.5 s). As a result, the buoyancy driven advection becomes dominant and the fluid particles descend downward forming a single vortex flow with maximum velocity being localized at the central core.

As the evaporation process progress, the buoyancy driven convection elevate the thermal diffusion process inside the liquid droplet. As a result, the temperature distribution becomes more uniform at intermediate stages (as observed at $t = 1.1$ s). This phenomenon ultimately alleviates the driving gradient for buoyancy mechanism. Also, the interfacial temperature gradient at this stage is too weak to stimulate Marangoni advection. As a result, the strength of internal circulation velocity at this intermediate stage ($t = 1.1$ s) is greatly reduced compared to early stages. Also, it can be mentioned that the continuous evaporative cooling along with the internal advection gradually leads to nearly uniform temperature distribution inside the droplet with the progressing evaporation time. In such cases, although the buoyancy effects become negligible, steep thermal gradient is induced at liquid–vapour

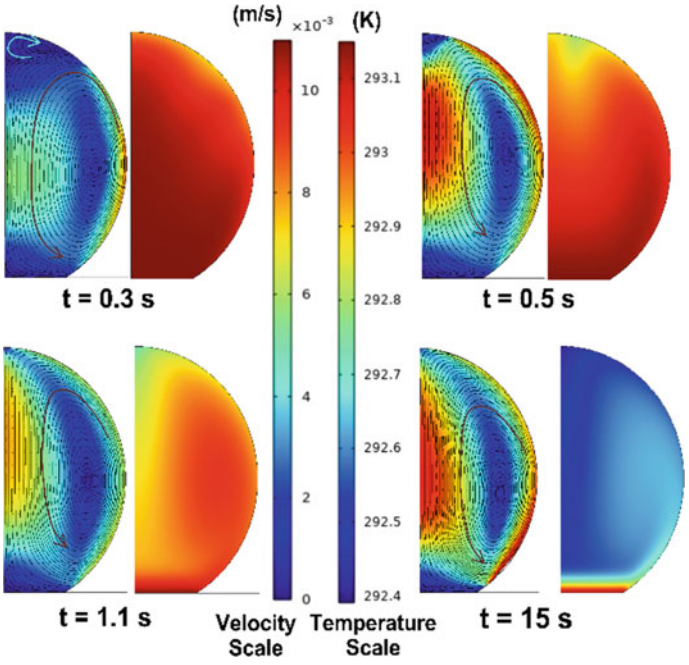

Fig. 4 Temporal evolution of the velocity field and corresponding temperature distribution inside a sessile droplet evaporating over SH surfaces ($\theta_0 = 150°$)

interface near the peripheral region (as noticed at $t = 15$ s). This condition ultimately set off thermal Marangoni advection thus forming single recirculation flow (one vortex pattern) inside the droplet.

4.2 Influence of Contact Angle on the Internal Circulation Velocity and Temperature

In this subsection, we portray the transient thermal response and internal circulation velocity of the evaporating droplets as a whole for different contact angles. Figure 5 illustrates the role of initial contact angle on the temporal evolution of overall temperature (T_a) and internal circulation velocity (V_a) of evaporating droplets. It can be noticed that there are several peaks and valleys in the velocity plot on hydrophilic surfaces. This is mainly due to the formation and evolution of localized circulation cells at different locations. On SH surfaces, the circulation velocity initially reaches to a local peak value followed by a step decrease at the intermediate stage ($t = 1.1$ s) and then gradually increases to a stable value with the progressing evaporation time. This behaviour may be attributed to the initial dominance of buoyancy force followed by alleviation of same as discussed earlier. Finally, at successive stages, thermal gradient near the contact line becomes significant thereby manifests higher velocity due to Marangoni flow. Also, it is noted that the velocity scale is increased in a consistent manner with the increase in contact angle. On SH surfaces the overall circulation velocity becomes almost an order of magnitude higher as compared to the hydrophilic surfaces.

The overall temperature (T_a) plot shows consistently decreasing trend at initial stages and finally reaches stable state with progressing time (see Fig. 5) for different contact angles of the evaporating droplets. This stable state is reached at much early stages for the hydrophilic surfaces compared to the SH surface. This is mainly due to large heat conduction path inside droplet on SH surfaces which delays stable temperature distribution inside the droplet. Also, the overall stable temperature for the SH surface is much lower than the hydrophilic case. This is mainly due to altered geometry of the droplet over these surfaces. For the hydrophilic surface, the large solid–liquid interfacial area and small droplet height (i.e., conduction path) cause higher overall temperature inside the droplet. Now for an identical volume the droplet placed on SH surfaces the maximum height of liquid column is increased with a simultaneous decrease in solid–liquid contact area. These conditions ultimately reduce the overall stable temperature of the bulk fluid inside droplet.

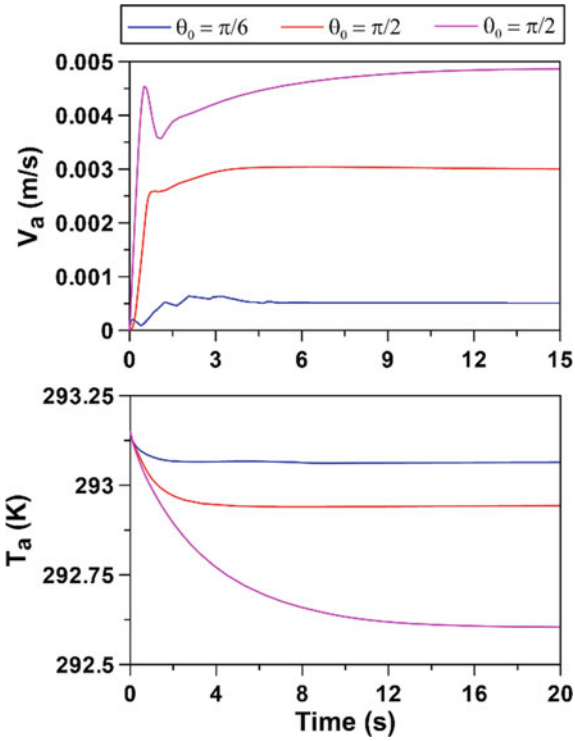

Fig. 5 Transient evolution of the overall internal circulation velocity and temperature variation inside sessile droplets for different contact angles

5 Conclusions

In present study we numerically probe the temporal evolution of internal hydrodynamics and temperature distribution profile of drying sessile droplets. A transient evaporation model based on ALE framework is employed for this purpose. We vary contact angle and other geometrical parameters keeping the volume of droplet constant to understand the influence of wettability of underlying substrate. The key insights are given as:

- On hydrophilic surfaces multiple vortices are formed at the transient stage due to non-uniform evaporative flux across liquid–vapour interface. This cause uneven evaporative cooling which set off thermal Marangoni and buoyancy driven advection inside droplet. Eventually, as temperature distribution across liquid–vapor interface becomes monotonic a single large recirculation vortex is formed from the peripheral region to the apex.
- For SH surfaces, the buoyancy effect becomes dominant at initial stages that cause single large recirculating flow encompassing the whole liquid domain inside the droplet. Finally at latter stages, as the temperature field reaches a nearly uniform state the Marangoni effect predominates over buoyancy forces.

- The overall temperature inside the droplet is significantly lower for SH surface due to large conduction path. This condition cause strong thermal gradient across the droplet interface near periphery that set off Marangoni advection. As result, the velocity scale is obtained as an order of magnitude higher for the SH surfaces as compared to hydrophilic surfaces.

References

1. Tardif R, Rasmussen RM (2010) Evaporation of nonequilibrium raindrops as a fog formation mechanism. J Atmos Sci 67(2):345–364
2. Ucar IO, Erbil HY (2012) Use of diffusion controlled drop evaporation equations for dropwise condensation during dew formation and effect of neighboring droplets. Colloids Surf, A 411:60–68
3. Park J, Moon J (2006) Control of colloidal particle deposit patterns within picoliter droplets ejected by ink-jet printing. Langmuir 22(8):3506–3513
4. Yu Y, Zhu H, Frantz JM, Reding ME, Chan KC, Ozkan HE (2009) Evaporation and coverage area of pesticide droplets on hairy and waxy leaves. Biosyst Eng 104(3):324–334
5. Lee S, Kim DI, Kim YY, Park SE, Choi G, Kim Y, Kim HJ (2017) Droplet evaporation characteristics on transparent heaters with different wettabilities. RSC Adv 7(72):45274–45279
6. Karlsson S, Rasmuson A, Björn IN, Schantz S (2011) Characterization and mathematical modelling of single fluidised particle coating. Powder Technol 207(1–3):245–256
7. Picknett RG, Bexon R (1977) The evaporation of sessile or pendant drops in still air. J Colloid Interface Sci 61(2):336–350
8. Bormashenko E, Musin A, Zinigrad M (2011) Evaporation of droplets on strongly and weakly pinning surfaces and dynamics of the triple line. Colloids Surf, A 385(1–3):235–240
9. Sefiane K, Wilson SK, David S, Dunn GJ, Duffy BR (2009) On the effect of the atmosphere on the evaporation of sessile droplets of water. Phys Fluids 21(6):062101
10. Paul A, Dhar P (2022) Interactive evaporation of neighboring pendant and sessile droplet pair. J Heat Transfer 144(12):121603
11. Paul A, Khurana G, Dhar P (2021) Substrate concavity influenced evaporation mechanisms of sessile droplets. Phys Fluids 33(8):082003
12. Paul A, Dhar P (2021) Evaporation kinetics of sessile droplets morphed by substrate curvature. Phys Fluids 33(12):122010
13. Paul A, Dash RK, Dhar P (2023) Phenomenology and kinetics of sessile droplet evaporation on convex contours. Int J Therm Sci 187:108194
14. Dunn GJ, Wilson SK, Duffy BR, David S, Sefiane K (2009) The strong influence of substrate conductivity on droplet evaporation. J Fluid Mech 623:329–351
15. Deegan RD, Bakajin O, Dupont TF, Huber G, Nagel SR, Witten TA (1997) Capillary flow as the cause of ring stains from dried liquid drops. Nature 389(6653):827–829
16. Al-Sharafi A, Yilbas BS, Sahin AZ, Ali H, Al-Qahtani H (2016) Heat transfer characteristics and internal fluidity of a sessile droplet on hydrophilic and hydrophobic surfaces. Appl Therm Eng 108
17. Dhar P, Khurana G, Anilakkad Raman H, Jaiswal V (2019) Superhydrophobic surface curvature dependence of internal advection dynamics within sessile droplets. Langmuir 35(6):2326–2333
18. Kumar S, Medale M, Brutin D (2022) Numerical model for sessile drop evaporation on heated substrate under microgravity. Int J Heat Mass Transf 195:123150
19. Dhar P, Jaiswal V, Chate H, Maganti LS (2020) Control and modulation of droplet vaporization rates via competing ferro-and electro-hydrodynamics. arXiv preprint arXiv:2006.00750
20. Maatar A, Chikh S, Ait Saada M, Tadrist L (2015) Transient effects on sessile droplet evaporation of volatile liquids. Int J Heat Mass Transf 86:212–220

21. Chen YH, Hu WN, Wang J, Hong FJ, Cheng P (2017) Transient effects and mass convection in sessile droplet evaporation: the role of liquid and substrate thermophysical properties. Int J Heat Mass Transf 108:2072–2087
22. Chen Y, Hong F, Cheng P (2020) Transient flow patterns in an evaporating sessile drop: a numerical study on the effect of volatility and contact angle. Int Commun Heat Mass Transfer 112:104493
23. Yang K, Hong F, Cheng P (2014) A s coupled numerical simulation of sessile droplet evaporation using arbitrary Lagrangian-Eulerian formulation. Int J Heat Mass Transf 70:409–420
24. Sobac B, Brutin D (2012) Thermal effects of the substrate on water droplet evaporation. Phys Rev E Stat Nonlinear Soft Matter Phys 86(2 Pt 1):021602